Photodynamic Therapy Using Talaporfin Sodium and Semiconductor Laser Induces Dose and Time Dependent Cytocidal Effect for Human Glioma Derived Stem Cells

Megumi Ichikawa , Jiro Akimoto * , Srivalleesha Mallidi , Hiroaki Wakimoto , Michihiro Kohno , Tayyaba Hasan

Posted Date: 12 June 2025

doi: 10.20944/preprints202506.1080.v1

Keywords: talaporfin sodium; photodynamic therapy; glioma stem cells; apoptosis; reactive oxygen species

 doi:10.20944/preprints202506.1080.v1

Article

Photodynamic Therapy Using Talaporfin Sodium and Semiconductor Laser Induces Dose and Time Dependent Cytocidal Effect for Human Glioma Derived Stem Cells

Megumi Ichikawa [1,2], Jiro Akimoto [3,*], Srivalleesha Mallidi [2,4], Hiroaki Wakimoto [5], Michihiro Kohno [3] and Tayyaba Hasan [2,6]

[1] Department of Neurosurgery, Tokyo Medical University Ibaraki Medical Center, Ibaraki, Japan
[2] Wellman Center for Photomedicine, Massachusetts General Hospital, Harvard Medical School, Boston, Massachusetts, USA
[3] Department of Neurosurgery, Tokyo Medical University, Tokyo, Japan
[4] Department of Biomedical Engineering, Tufts University, Medford, Massachusetts, USA
[5] Brain Tumor Research Center and Molecular Neurosurgery Laboratory, Department of Neurosurgery, Massachusetts General Hospital, Harvard Medical School, Boston, Massachusetts, USA
[6] Division of Health Sciences and Technology, Harvard University and Massachusetts Institute of Technology, Cambridge, Massachusetts, USA
* Correspondence: jiroaki@gmail.com; Tel.: +81-3-3342-6111 (ext 5773); Fax: +81-3-3340-4285

Abstract: One of the key factors contributing to the poor prognosis of glioblastoma is the treatment resistance of glioma stem cells (GSCs). In this study, the authors used MGG8, a patient-derived GSC line established from human glioblastoma, to evaluate the efficacy of photodynamic therapy (PDT) using talaporfin sodium (NPe6)—a second-generation photosensitizer—and a semiconductor laser approved for clinical use in Japan. Under favorable oxygenation conditions, NPe6-PDT induced a dose- and fluence-dependent suppression of mitochondrial metabolic activity in MGG8 cells, mirroring responses previously observed in conventional glioblastoma cell lines. A similar pattern of cell death was noted, with both apoptosis and necrosis occurring in a time-dependent manner. Secondary reactive oxygen species (ROS) levels were also increased following PDT, indicating sustained intracellular oxidative stress. Given that GSC resistance is partly attributed to hypoxic microenvironments that diminish treatment-induced oxidative damage, these findings suggest that strategies to enhance tissue oxygenation could improve the therapeutic efficacy of NPe6-PDT against GSCs. This study represents the first experimental system to investigate NPe6-PDT in patient-derived GSCs and provides a foundation for future translational research.

Keywords: talaporfin sodium; photodynamic therapy; glioma stem cells; apoptosis; reactive oxygen species

Introduction

Glioblastoma (GBM) is an aggressive brain tumor for which the current standard of care includes maximal safe surgical resection followed by adjuvant chemoradiotherapy. Despite these efforts, most patients experience tumor recurrence—typically within two years—and ultimately succumb to the disease [1–3]. Notably, 80–90% of recurrences occur locally, arising from residual tumor cells that evade initial resection and cytotoxic treatments [2,4]. These residual cells, which cannot be fully eliminated even with advanced surgical and adjuvant techniques, are thought to include glioma stem cells (GSCs)—a treatment-resistant subpopulation capable of initiating tumor regrowth [4–6].

GSCs were first identified in 2004 as undifferentiated, tumor-initiating cells within glioma tissue [7,8]. Since then, they have been recognized as a key contributor to GBM recurrence and resistance to

 doi:10.20944/preprints202506.1080.v1

therapy. Numerous studies have demonstrated that GSCs are highly resistant to both radiotherapy and chemotherapy, making them a critical barrier to curative treatment [9]. As a result, there is growing interest in developing strategies to specifically target or suppress the function of GSCs in order to improve patient outcomes.

The authors have demonstrated that PDT using the second-generation photosensitizer talaporfin sodium, mono-L-aspartyl chlorin e6 (NPe6), and its excitation laser induces apoptosis and necrosis in glioblastoma cells [10–14]. In clinical cases, intraoperative application of PDT to the resection cavity after maximum safe resection significantly prolonged progression-free survival (PFS) and overall survival (OS) [15–17]. PDT is currently recognized in Japan as an effective and safe treatment for primary malignant brain tumors and is covered by national health insurance [15]. However, even in previous in vitro studies, complete cell death was not observed in various standard glioma cell lines [10,11,14]. Although it prolonged PFS in clinical cases [17,18], approximately 60% of patients eventually developed local recurrence [18]. In other words, there are glioma cells that are resistant to PDT in both in vitro experiments and clinical settings. It is therefore highly likely that these cells contribute to tumor regrowth, and that complete elimination of GSCs, which are characterized by treatment resistance, may be difficult even with PDT.

In the present study, the authors used a GSC line established from human brain tumor tissue by their collaborators to investigate whether NPe6-mediated PDT exerts a cytocidal effect on GSCs. Furthermore, the authors compared 5-aminolevulinic acid (5-ALA)-based PDT, which has been developed primarily in Europe and the United States [19,20], with NPe6-mediated PDT to evaluate their respective capacities to generate secondary reactive oxygen species (ROS).

Materials and Methods

MGG8 Glioma Stem Cell Line and Spheroid Culture Conditions

MGG8 is a patient-derived GSCs line that HW's group established at Massachusetts General Hospital [21,22]. It was derived from the surgical specimen of a patient with a large, irregular, ring-enhancing mass on gadolinium-enhanced T1-weighted magnetic resonance imaging (MRI), consistent with invasive glioblastoma in the left temporal lobe [21]. Histologically, the tumor displayed typical glioblastoma features, including microvascular proliferation and pseudopalisading necrosis, but also contained highly undifferentiated components resembling primitive neuroectodermal tumor (PNET)-like elements [21]. The MGG8 cell line, derived from the initial culture of the resected tissue, was transplanted into the mouse brain, where it recapitulated a glioblastoma containing a PNET-like component similar to the original tumor [22]. MGG8 is characterized by activation of the PTEN/PI3K pathway and exhibits MGMT promoter methylation. Its genomic profile includes amplification of MYCN (2p24.3), PDGFRA (4q12), and MDM2 (12q15), along with homozygous deletion of CDKN2A/B (9p21.3) [22].

MGG8 cells were cultured as spheroids in EF20 medium, which consists of Neurobasal medium (Invitrogen Inc., Carlsbad, CA) supplemented with L-glutamine (3 mM; Mediatech Inc., Manassas, VA), B27 supplement (Invitrogen Inc., Carlsbad, CA), N2 supplement (Invitrogen Inc., Carlsbad, CA), heparin (2 μg/mL; Sigma-Aldrich Co., St. Louis, MO), EGF (20 ng/mL; R&D Systems Inc., Minneapolis, MN), and FGF2 (basic FGF, 20 ng/mL; PeproTech Inc., Cranbury, NJ).
Spheroids were dissociated using the NeuroCult™ Chemical Dissociation Kit (StemCell Technologies, Cambridge, MA) during passaging or prior to cell analysis.

Photosensitizers Reagents

Talaporfin sodium (NPe6) was provided by Meiji Seika Pharma Co., Ltd. (Tokyo, Japan), and 5-Aminolevulinic acid hydrochloride (5-ALA) was obtained from Sigma-Aldrich Co. (St. Louis, MO).

 doi:10.20944/preprints202506.1080.v1

Quantification of NPe6 Uptake in MGG8 Cells

MGG8 cells were seeded at 1 × 10^5 cells per 35-mm dish in RPMI 1640 medium supplemented with 10% fetal bovine serum (FBS) and cultured at 37 °C in a 5% CO_2 atmosphere for 3 days. After incubation, the cells were washed with calcium- and magnesium-free Dulbecco's phosphate-buffered saline [DPBS (–)] and incubated with 0–100 μM NPe6 for either 1 hour or 4 hours under dark conditions in 10% FBS–RPMI 1640. After incubation with NPe6, the cells were washed once with in DPBS (–), and NPe6-positive fluorescent cells were quantified by flow cytometry (excitation: 405 nm; emission: 660 nm).

Photodynamic Therapy Protocol for MGG8 Cells

MGG8 cells were seeded at 1 × 10^5 cells per 35-mm dish and cultured in RPMI 1640 medium supplemented with 10% fetal bovine serum (FBS) (10% FBS–RPMI 1640) at 37 °C in 5% CO_2 atmosphere for 3 days. After incubation, the cells were washed with DPBS (–), and the GSCs spheroid cultures were incubated with either 0–60 μM NPe6 for 1 hour or 0–1000 μM 5-ALA for 24 hours in 10% FBS–RPMI 1640. Following NPe6 incubation, the cells were washed with DPBS (–), immersed in fresh 10% FBS–RPMI 1640, and subjected to laser irradiation. PDT protocols were as follows: for NPe6-PDT, cells were irradiated with a 670 nm semiconductor laser (Intense Co., Cedar Knolls, NJ) at a power density of 50 mW/cm², delivering a total light dose of 0–10 J/cm²; for 5-ALA-PDT, cells were irradiated with a 635 nm laser under the same power and fluence conditions.

Assessment of Relative Mitochondrial Metabolic Activity

After PDT, the cells were incubated for 3 days in 10% FBS-RPMI 1640. They were seeded into a 96-well culture plates at 1 × 10^5 cells per well, and relative metabolic activity was measured using MTT assay (Sigma-Aldrich, St Louis, MO) with microplate reader.

The MTT assay was used to evaluate mitochondrial metabolic activity as an indicator of cytotoxic response. Although it is often used as a proxy for cell viability, the MTT assay does not directly measure cell death or long-term survival.

Assessment of Secondary Reactive Oxygen Species (ROS) Production

Dissociated MGG8 cells were seeded at 1 × 10^5 cells per 35-mm dish and cultured in 10% FBS–RPMI 1640 for 3 days. Following incubation, the cells were washed with DPBS (–), then incubated with either 30 μM NPe6 for 1 hour or 60 μM 5-ALA for 24 hours in 10% FBS–RPMI 1640. After incubation, cells treated with NPe6 were irradiated with a 670 nm semiconductor laser at a total light dose of 5 J/cm² (laser power: 50 mW/cm²), and cells treated with 5-ALA were irradiated with a 635 nm semiconductor laser under the same conditions. Following PDT, the cells were washed with DPBS (–). Immediately (0 h) and 3 hours (3 h) after PDT, the cells were incubated with fresh culture medium containing 25 μM 2′,7′-dichlorodihydrofluorescein diacetate (DCFH-DA; Life Technologies Co., Carlsbad, CA) for 30 minutes. After incubation, the cells were washed once with DPBS (–) and transferred to a 24-well microplate. DCF fluorescence intensity was measured using fluorescence spectroscopy. Intracellular ROS levels were expressed as DCF fluorescence intensity normalized to the total protein content (mg), as determined using the BCA Protein Assay Kit (Thermo Fisher Scientific Inc., Waltham, MA). To avoid artifactual oxidation of the DCFH probe during light exposure, DCFH-DA was added immediately after irradiation. This post-irradiation protocol is intended to detect sustained oxidative stress caused by long-lived ROS species (e.g., hydrogen peroxide, lipid peroxides), rather than short-lived primary ROS such as singlet oxygen or hydroxyl radicals.

Quantification of Apoptosis and Necrosis by Flow Cytometry

Dissociated MGG8 cells were seeded at 1 × 10^5 cells per 35-mm dish and cultured in 10% FBS–RPMI 1640 for 3 days. After incubation, the cells were washed with DPBS (–), and incubated with 60

 doi:10.20944/preprints202506.1080.v1

μM NPe6 for 1 hour in 10% FBS–RPMI 1640. Following PDT treatment, the cells were washed once with DPBS (–) and cultured again in 10% FBS–RPMI 1640. After 4 or 24 hours of incubation, the cells were transferred to 96-well plate and stained with Live/Dead Fixable Near-IR Dead Cell Stain (Life Technologies Co., Carlsbad, CA). After removal of the supernatant, the cells were further stained with Annexin V–PE conjugate (Life Technologies Co., Carlsbad, CA). The stained cells were then transferred to flow cytometry tubes, and the rates of apoptosis and necrosis were analyzed by flow cytometry.

Statistical Analysis

The data are presented as mean ± standard deviation (SD) and were analyzed for statistical significance using analysis of variance (ANOVA) and Student's *t*-test. A *P* value less than 0.05 was considered statistically significant.

Results

Uptake of NPe6 by MGG8

As shown in Figure 1A, NPe6 uptake by MGG8 cells increased over time. After a 4-hour exposure to 50 μM NPe6, approximately 70% of the cells were NPe6-positive, compared to a lower uptake at 1 hour.

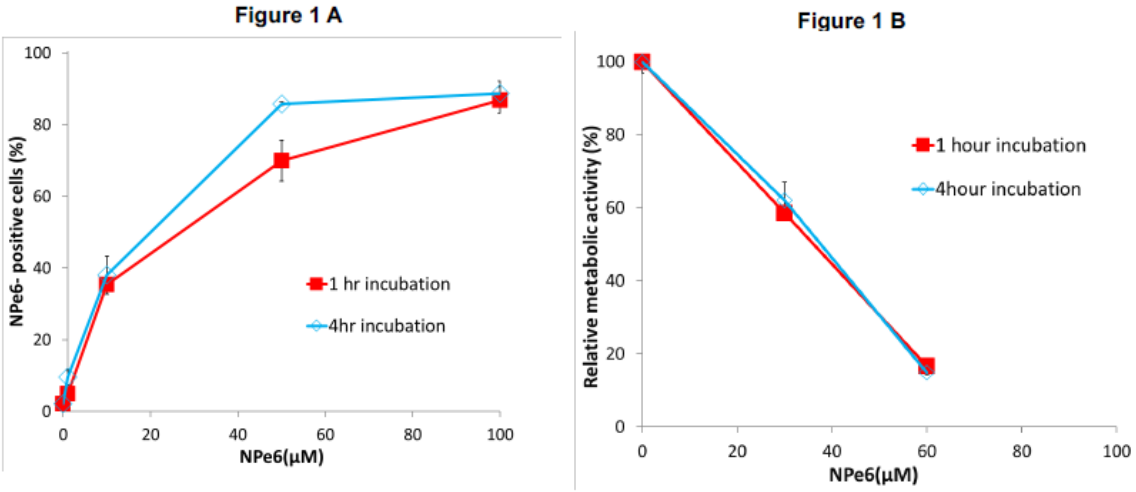

Figure 1. Intracellular uptake and early metabolic Effects of NPe6 in MGG8 cells. (**A**) Intracellular accumulation of NPe6 after 1-hour and 4-hour incubation at various concentrations was assessed by flow cytometry. The proportion of NPe6-positive fluorescent cells increased with longer incubation times, indicating efficient internalization of the photosensitizer. (**B**) Following incubation with NPe6 for 1 or 4 hours, cells were irradiated with a 670 nm laser at 5 J/cm² and 50 mW/cm². Metabolic activity was measured 3 days post-PDT using the MTT assay, which reflects NAD(P)H-dependent mitochondrial reductase function and serves as an early indicator of photodynamic cytotoxic stress.

Effect of NPe6 Incubation Time on Early Metabolic Response in MGG8

As shown in Figure 1B, the relative metabolic activity of MGG8 cells measured three days after NPe6-PDT treatment (670 nm wavelength, 50 mW/cm², 5 J/cm²) was nearly identical between the 1-hour and 4-hour incubation conditions, despite differences in NPe6 uptake. These results demonstrate that NPe6 is biologically active upon internalization and helped determine appropriate incubation and irradiation parameters for subsequent experiments, which were performed using a 1-hour incubation period with NPe6.

 doi:10.20944/preprints202506.1080.v1

Dose- and Fluence-Dependent Changes in Early Mitochondrial Metabolic Activity in MGG8 Following NPe6-PDT

Figure 2 shows the differences in relative metabolic activity of MGG8 cells depending on the energy density of 670 nm, 50 mW/cm² laser light, following a 1-hour incubation with various concentrations of NPe6. Incubation with NPe6 alone, without subsequent laser exposure, did not reduce metabolic activity at any tested concentration. A significant decrease in metabolic activity—indicative of a cytotoxic effect—was observed when cells were irradiated after 1-hour incubation with NPe6 at concentrations of 20 μM or higher. An irradiation energy of 5 J/cm² or more was considered appropriate for inducing this effect.

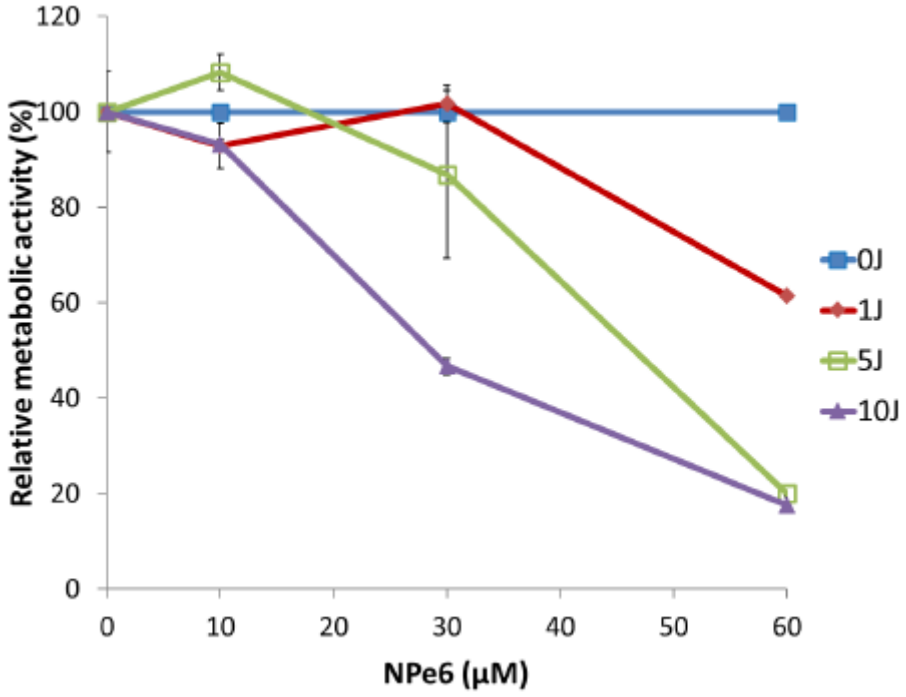

Figure 2. Dose- and fluence-dependent changes in early mitochondrial metabolic activity in MGG8 following NPe6-PDT. At both 5 J/cm² and 10 J/cm², relative metabolic activity decreased as the concentration of NPe6 increased. At concentrations of 10 μM or higher, the cytotoxic effect of NPe6-PDT was clearly dependent on both NPe6 dose and light fluence. MGG8 cells were incubated with NPe6 for 1 h. After replacing the medium, cells were irradiated with a 670 nm laser at a power density of 50 mW/cm². Mitochondrial metabolic activity was assessed by MTT assay three days post-irradiation.

The half maximal inhibitory concentration (IC_{50}) of NPe6 in PDT against MGG8 cells was determined to be 40 μM with 5 J/cm² irradiation and approximately 20–25 μM with 10 J/cm² irradiation. However, even at 60 μM NPe6 combined with 10 J/cm² irradiation, a residual population of cells retained measurable metabolic activity, indicating that the cytotoxic effect was not complete under these conditions.

Dose- and Fluence-Dependent Changes in Early Mitochondrial Metabolic Activity in MGG8 Following 5-ALA–PDT

Figure 3 shows the survival curves of MGG8 cells after exposure to 5-ALA at various doses for 24 h followed by laser irradiation of the 635 nm, 50 mW/cm² at various energy densities. When 5-ALA was administered without subsequent laser irradiation, no reduction in metabolic activity was observed. Similar patterns of decreased metabolic activity were seen following 5 J/cm² and 10 J/cm² irradiation in a dose-dependent manner with 5-ALA, although the curve for 1 J/cm² irradiation differed slightly from those at higher energy densities. The IC_{50} of 5-ALA was assessed to be roughly 230 μM after 24 hours of exposure to 5-ALA, followed by laser irradiation at 5 J/cm² or 10 J/cm². Even

 doi:10.20944/preprints202506.1080.v1

at higher concentrations, however, the cytotoxic effect was not complete: as with NPe6-PDT, approximately 20% of the metabolic activity of MGG8 cells remained after treatment with the maximum dose of 5-ALA and 10 J/cm² laser irradiation.

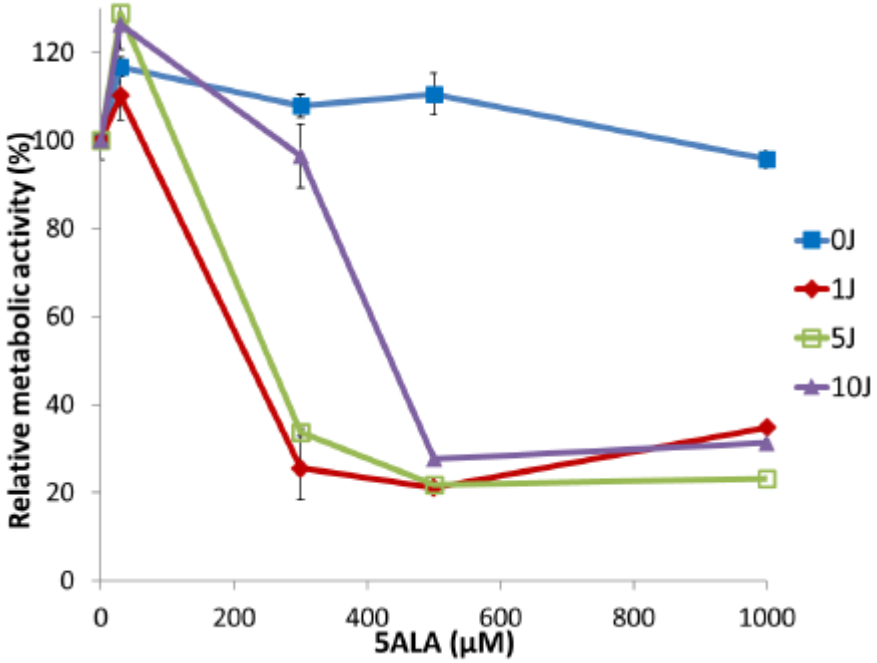

Figure 3. Dose- and fluence-dependent changes in early mitochondrial metabolic activity in MGG8 following 5-ALA-PDT. The IC_{50} of 5-ALA was approximately 230 μM under an irradiation dose of 5 J/cm². MGG8 cells were incubated with 5-ALA for 24 hours, washed with PBS, and subsequently irradiated using a 635 nm laser at a power density of 50 mW/cm². Mitochondrial metabolic activity was evaluated three days post-irradiation using the MTT assay.

Comparison of Secondary ROS Accumulation Induced by NPe6-PDT and 5-ALA–PDT

As shown in Figure 4, in the NPe6-PDT group, a strong ROS signal was observed immediately after PDT, with a relative reduction to about one-fifth after 3 h. In contrast, the ROS signal in the 5-ALA-PDT group was much lower than that of NPe6-PDT and remained relatively sustained over the 3-hour period. It should be noted that these measurements reflect long-lived oxidative products detected post-irradiation, and not real-time generation of short-lived ROS species.

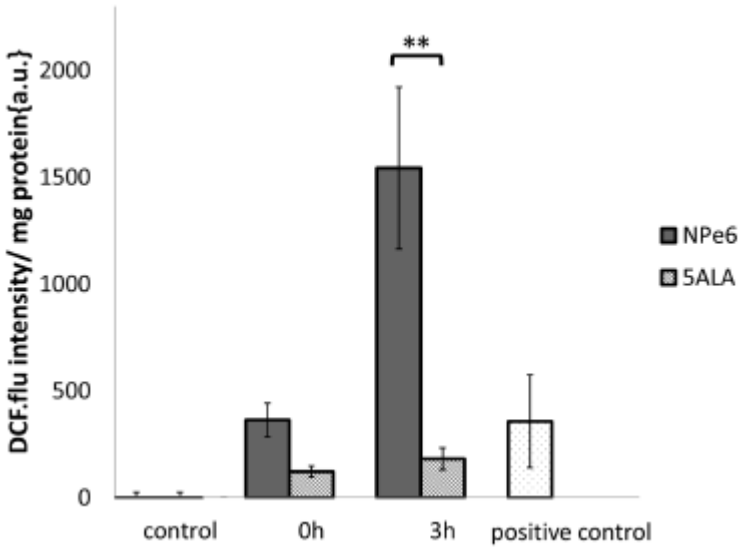

 doi:10.20944/preprints202506.1080.v1

Figure 4. Secondary ROS Accumulation following PDT. Cells were incubated with NPe6 (60 μM) for 1 hour or with 5-ALA (60 μM) for 24 hours, then washed with PBS and irradiated either at 670 nm (NPe6, 50 mW/cm²) or at 635 nm (5-ALA, 50 mW/cm²). DCFH-DA (10 μM) was applied after irradiation—either immediately (0 h) or 3 hours post-PDT (3 h)—and cells were incubated for 30 minutes before fluorescence measurement using a spectrophotometer. Because the probe was added post-irradiation, the observed DCF fluorescence reflects longer-lived secondary ROS (e.g., hydrogen peroxide, lipid peroxides) rather than short-lived primary ROS such as singlet oxygen or hydroxyl radicals. All groups were treated under identical conditions to enable valid comparative assessment of sustained oxidative stress induced by each PDT protocol. For positive controls, oxidative stress was induced using 10 mM H_2O_2.

Time-Dependent Apoptosis and Necrosis Induced by NPe6-PDT in MGG8 Cells

As shown in Figure 5, flow cytometry analysis revealed changes in the cell death pattern of MGG8 cells between 4 and 24 hours after PDT. The proportion of cells in the apoptotic fraction was 17% at 4 hours, decreasing to 7% at 24 hours. In contrast, the proportion of cells in the necrotic fraction increased from 42% at 4 hours to 63% at 24 hours.

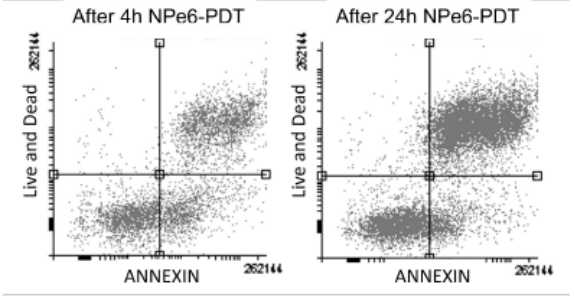

Fig.5 A

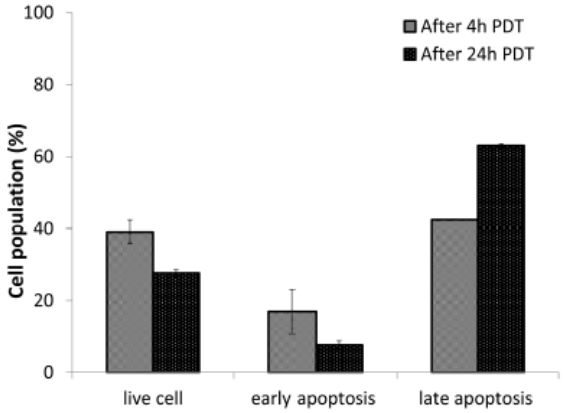

Fig.5 B

Figure 5. Time-dependent apoptosis and necrosis in MGG8 following NPe6-PDT. Cells were incubated with 30 μM NPe6 for 1 hour, and PDT treatment was performed at 5 J/cm² and 50 mW/cm². (A) At 4 and 24 hours after PDT, cells were stained with Annexin V and Live/Dead Fixable Near-IR stain (×100) and analyzed by flow cytometry to evaluate apoptosis. (B) Flow cytometry analysis revealed that the proportion of cells in the apoptotic fraction decreased from 17% at 4 hours to 7% at 24 hours, while the proportion of necrotic cells increased from 42% to 63%, indicating a temporal shift from apoptosis to necrosis after PDT.

Discussion

In the past, glioblastoma was referred to as *glioblastoma multiforme*, reflecting its highly heterogeneous pathological morphology—a complex mixture of tumor cells exhibiting various degrees of differentiation. However, since all cancers originate from a series of genetic mutations initiated in cancer stem cells, it is reasonable to consider that developing therapies targeting GSCs may offer the most effective strategy for eradicating glioblastoma. Yet, as research on cancer stem cells has advanced, their strong resistance to cell death and therapies has emerged as a major challenge.

The development of NPe6, a second-generation photosensitive chlorin derivative, and its application in PDT has offered renewed hope to glioblastoma treatment. NPe6 was developed by a Japanese company, and the authors were the first to introduce NPe6-based PDT as a therapeutic strategy for malignant brain tumors. Clinical studies have demonstrated that this approach significantly prolongs both median progression-free survival (mPFS) and median overall survival

 doi:10.20944/preprints202506.1080.v1

(mOS) in patients with glioblastoma [16–18]. This procedure was approved by the Japanese government 10 years ago as an adjunct to the standard treatment for glioblastoma, and it is now routinely performed at many medical institutions across Japan. However, even with the addition of PDT, tumor recurrence is inevitable, and patients succumb to the disease [18,23]. This indicates that PDT cannot eradicate all infiltrating tumor cells, and that a subpopulation of glioblastoma cells remains resistant to this therapy. Moreover, a closer examination of recurrence patterns following PDT reveals a higher frequency of distant recurrence and cerebrospinal fluid (CSF) dissemination compared to conventional therapy [18,23]. This may suggest that while PDT improves local tumor control and prolongs mPFS, it may also lead to relatively increased rates of distant relapse and CSF seeding. GSCs, which are believed to reside in the subventricular zone, may be particularly resistant to PDT [24–26]. Furthermore, there is emerging evidence that PDT may activate the proliferative and migratory capacities of treatment-resistant GSCs [26,27].

The authors investigated the cytotoxic response of NPe6-mediated PDT in MGG8, a GSC line established from a human glioblastoma patient, by assessing both early mitochondrial dysfunction and subsequent apoptotic or necrotic cell death in vitro. To evaluate whether GSCs exhibit greater resistance to PDT than conventional glioma cells, these responses were compared with previously published data from standard glioblastoma cell lines [10–14].

The IC_{50} values of NPe6 in glioma cell lines such as U251, A172, and T98G , as reported by Tsutsumi et al. [10] and malignant meningioma cell lines such as HKBMM and KMY-J reported by Ichikawa et al. [14], were comparable to the IC_{50} value observed in the MGG8 glioma stem cell line in the present study, approximately 25–30 μg/mL [10,13,14]. These results do not suggest that MGG8 is resistant to NPe6-PDT. The pattern of cell death induced by NPe6-PDT in MGG8 cells included both apoptosis and necrosis. Although the balance between these modes of cell death varied over time after treatment, the overall pattern was comparable to that observed in conventional glioma cell lines treated with NPe6-PDT [10–14]. The necroptosis reported by Miki et al. in malignant glioma cells treated with NPe6-PDT [11,13] was also observed in the GSC line MGG8. In summary, GSCs exhibited sensitivity to PDT comparable to that of standard glioma cell lines, suggesting that intraoperative PDT applied to the walls of the resection cavity after maximal tumor resection may contribute to the elimination of residual GSCs in clinical practice [15–18].

To assess early-phase cytotoxic responses to PDT, the authors used the MTT assay to evaluate dose- and fluence-dependent changes in mitochondrial metabolic activity. While MTT does not directly measure long-term survival or clonogenic potential, it offers a reproducible and quantitative readout of NAD(P)H-dependent mitochondrial reductase activity—an early cellular function that is highly sensitive to oxidative damage [28,29]. Given that PDT rapidly impairs mitochondrial function, decreases in MTT signal serve as biologically meaningful indicators of acute cytotoxic stress.

This approach is consistent with widely accepted PDT methodologies, in which MTT or similar metabolic assays are commonly employed to determine optimal photosensitizer concentrations and light fluences prior to conducting mechanistic analyses [30,31]. In the authors' study, metabolic profiling using the MTT assay (Figures 2 and 3) clarified the dose- and fluence-dependent extent of mitochondrial dysfunction in GSCs and served as the basis for selecting treatment parameters. In summary, Figures 2 and 3 were indispensable in establishing that PDT exerts dose-responsive, biologically relevant cytotoxic effects in patient-derived GSCs—an essential step for justifying the experimental parameters used throughout this study.

Recognizing the interpretive limitations of metabolic assays alone, the authors confirmed that MTT-detected metabolic suppression was associated with bona fide cell death by incorporating Annexin V/PI staining as a second-tier evaluation. This two-tiered strategy aligns with best practices in PDT research and strengthens the causal interpretation of cytotoxicity by functionally linking mitochondrial dysfunction to specific cell death pathways [30,32–34]. To further validate this link, the authors analyzed Annexin V/PI profiles after PDT (Figure 5), which revealed that the metabolic suppression measured by MTT corresponded to apoptosis and necrosis. Specifically, a temporal shift was observed, from ~17% apoptotic and ~42% necrotic cells at 4 h post-irradiation to ~7% and ~63%

 doi:10.20944/preprints202506.1080.v1

at 24 h. These findings demonstrate that MTT-measured loss of metabolic activity reflects a biologically meaningful progression of PDT-induced cytotoxicity in patient-derived GSCs.

The DCFH-DA used in this experiment primarily detects intracellular ROS in vitro, but its interpretation requires careful consideration of experimental timing and chemical specificity. DCFH is not selective for singlet oxygen and can be oxidized by a range of reactive species, including thiol radicals, nitrogen dioxide, peroxynitrite, and redox-active proteins such as cytochrome c [35–37]. To minimize the risk of nonspecific photooxidation of the probe during PDT—especially under intense light exposure and in the presence of photosensitizers— the authors deliberately added DCFH-DA after irradiation. This approach has been adopted in previous PDT studies to avoid false-positive signals arising from artifactual probe oxidation [38–40].

As a result, the DCF fluorescence measured in our study should not be interpreted as a direct indicator of short-lived ROS (e.g., singlet oxygen, hydroxyl radicals), which decay within microseconds and are no longer present at the time of probe addition. Instead, the detected signal likely reflects longer-lived, secondary oxidative species such as hydrogen peroxide and lipid peroxides, which persist and propagate cellular stress after the primary photochemical reactions [41–43]. Although this design does not enable real-time detection of ROS during irradiation, it captures biologically relevant downstream oxidative stress and allows for valid relative comparisons between treatment groups.

Indeed, significant differences in ROS levels were observed between NPe6-PDT and 5-ALA-PDT, which may be partly attributed to the higher singlet oxygen quantum yield of NPe6 ($\Phi = 0.77$) compared to protoporphyrin IX ($\Phi = 0.56$) [44]. Additionally, prior reports suggest that DCFH-detectable ROS accumulate rapidly in lysosomes after NPe6-PDT, reflecting subcellular localization of oxidative events [45].

To further improve specificity and temporal resolution in future studies, the authors plan to incorporate real-time ROS probes such as Singlet Oxygen Sensor Green (SOSG) or hydroxyphenyl fluorescein (HPF) to directly monitor primary ROS generation during PDT. Nonetheless, the authors believe the current assay design provides meaningful insight into sustained oxidative stress, which is a key component of PDT-induced cytotoxicity in glioma stem cells.

One major challenge is the treatment resistance characteristic of GSCs. Cancer tissues often experience chronic hypoxia due to an imbalance between oxygen supply and demand, and it is believed that the more severe the hypoxia, the more readily cancer cells undergo de-differentiation and infiltrate normal brain tissue in search of oxygen [46–48]. In addition, the generation of free radicals—the principal cytotoxic mechanism of both chemotherapy and radiotherapy—is impaired under hypoxic conditions [48,49]. GSCs are thought to reside preferentially in these hypoxic tumor niches, particularly in infiltrative tumor regions that remain after surgical resection. These residual GSCs are believed to contribute to tumor recurrence by initiating new glioblastomas with varying degrees of differentiation [47,48].

On the other hand, the primary mechanism of PDT, as studied by the authors, involves the excitation of photosensitizers accumulated in tumor cells by specific wavelengths of light. As the excited photosensitizers return to their ground state, they transfer energy to molecular oxygen, producing highly cytotoxic singlet oxygen, which induces tumor cell death [15]. In other words, the efficacy of PDT depends on the concentration of the photosensitizer, the energy density of the irradiated light, and the availability of dissolved oxygen within the tissue [15]. A key question, however, is whether sufficient singlet oxygen can be generated to achieve cytotoxicity in hypoxic tumor regions, where GSCs are typically located. This experimental system was conducted in vitro under the normal culture conditions of 21% oxygen concentration, which is naturally an environment where singlet oxygen is easily generated. Therefore, the extent to which the observed PDT effects on GSCs reflect in vivo outcomes remains uncertain. To more accurately evaluate the effectiveness of PDT against GSCs, a hypoxia-adapted in vitro system should be established, with careful control and quantification of oxygen concentration. Nonetheless, the current findings suggest that PDT may effectively induce cell death in GSC as long as sufficient oxygen is available. Supporting this concept,

 doi:10.20944/preprints202506.1080.v1

Germany's group has conducted clinical studies on interstitial PDT (i-PDT) using 5-ALA as a photosensitizer [50,51]. In their approach, 100% oxygen is administered via mechanical ventilation to enhance ROS production during treatment [50,51]. This suggests that intraoperative oxygen enrichment may be a critical strategy to enhance PDT efficacy against GSCs, although it carries potential risks such as acute renal failure and myocardial ischemia [52].

Although the authors successfully demonstrated the validity of the NPe6-PDT methodology in terms of secondary ROS production for future GSC-targeted therapy, generating sufficient ROS in the hypoxic microenvironment where GSCs reside remains a challenge. To enhance PDT efficacy under such conditions, it is essential to increase the level of dissolved oxygen in the tissue. One potential strategy is intraoperative administration of high-concentration oxygen. The authors intend to further investigate optimal methods for oxygenating GSCs to improve PDT outcomes, while carefully weighing the risk of adverse effects.

Conclusion

This study presents the first experimental evaluation of PDT using NPe6 in patient-derived GSCs, a population central to treatment resistance and recurrence in glioblastoma. Using the MGG8 GSC line established from human glioblastoma tissue, the authors demonstrated that NPe6-PDT induces suppression of mitochondrial metabolic activity in a dose- and fluence-dependent manner, and elicits both apoptotic and necrotic cell death in a time-dependent fashion under normoxic conditions—responses comparable to those observed in standard glioma cell lines. Secondary ROS levels were elevated after irradiation, indicating sustained intracellular oxidative stress, although short-lived ROS were not directly measured. These findings suggest that NPe6-PDT can be effective against GSCs under sufficient oxygenation and that strategies to enhance tissue oxygenation could further improve its therapeutic efficacy by facilitating singlet oxygen generation in hypoxic tumor regions. The authors believe these results provide a novel foundation for optimizing PDT strategies targeting therapy-resistant GSCs in glioblastoma.

Author Contributions: Conceptualization, M.I., S.M. and J.A.; Data curation, M.I. and J.A.; Investigation, M.I., T.H. and J.A.; Methodology, M.I., S.M., H.W. and J.A.; Resources, M.I., H.W. and Meiji Seika Pharma Co., Ltd.; Validation, T.H. and J.A.; Writing – original draft, M.I. and J.A.; Writing – review & editing, S.M., T.H. and M.K. All authors have read and agreed to the published version of the manuscript.

Funding: There is no funding related to this paper.

Data Availability Statement: The datasets used and/or analyzed during the current study **are** available from the corresponding author on reasonable request.

Ethics Approval: There are no ethical regulations for the experiments described in this article.

Conflicts of Interest: The authors declare that they have no conflicts of interest and no personal or institutional financial interests regarding any of the drugs, materials, or devices described in this article.

Reference

1. Stupp R, Mason WP, van den Bent MJ, Weller M, Fisher B, Taphoorn MJB, Belanger K, Brandes AA, Marosi C, Bogdahn U, Curschmann J, Janzer RC, Ludwin SK, Gorlia T, Allgeier A, Lacombe D, Cairncross JG, Eisenhauer E, Mirimanoff RO. Radiotherapy plus concomitant and adjuvant temozolomide for glioblastoma. *NEJM*. 2005; 10: 987-996.
2. Sales AH, Beck J, Schnell O, Fung C, Meyer B, Gempt J. Surgical treatment of glioblastoma: state-of-the-art and future trend. *J Clin Med.* 2022; 11: 5354;https://doi.org/10.3390/jcm11185354
3. Jusue-Torres I, Lee J, Germanwala AV, Burns T, Parney IF. Effect of extent of resection on survival of

 doi:10.20944/preprints202506.1080.v1

patients with glioblastoma, IDH Wild-type, WHO Grade 4 (WHO 2021): systematic review and meta-analysis. *World Neurosurg*. 2023; 171: e524-e532. doi:10.1016/j.wneu.2022.12.052

4. Keles GE, Lamborn KR, Chang SM, Prados MD, Berger MS. Volume of residual disease as a predictor of outcome in adult patients with recurrent supratentorial glioblastomas multiforme who are undergoing chemotherapy. *J Neurosurg*. 2004; 100: 41-46.
5. Tamura M, Aoyagi M, Wakimoto H, Ando N, Nariai T, Tamamoto M, Ohno K. Accumulation of CD133-positive glioma cells after high-dose irradiation by gamma knife surgery plus external beam radiation. *J Neurosurg*. 2010; 113(2): 310-8
6. Tamura M, Aoyagi M, Ando N, Ogishima T, Wakimoto H, Yamamoto M, Ohno K. Expansion of CD133-positive glioma stem cells in recurrent de novo glioblastomas after radiotherapy and chemotherapy. *J Neurosurg*. 2013; 119(5): 1145-55.
7. Singh SK, Hawkins C, Clarke ID, Squire JA, Bayani J, Hide T, Henkelman RM, Cusimano MD, Dirks PB. Identification of human brain tumor initiating cells. *Nature*. 2004; 432(7015): 396-401
8. Singh SK, Clarke ID, Terasaki M, Bonn VE, Hawkins C, Squire J, Dirks PB. Identification of a cancer stem cell in human brain tumors. *Cancer Res*. 2003; 63(18): 5821-8
9. Altaner C. Glioblastoma and stem cells. *Neoplasma*. 2008; 55(5):369-74
10. Tsutsumi M, Miki Y, Akimoto J, Haraoka J, Aizawa K, Hirano K, Beppu M. Photodynamic therapy with talaporfin sodium induces dose-dependent apoptotic cell death in human glioma cell lines. *Photodiagnosis Photodyn Ther*. 2013;10(2):103-10. doi: 10.1016/j.pdpdt.2012.08.002. Epub 2012 Sep 25.PMID: 23769275
11. Miki Y, Akimoto J, Yokoyama S, Homma T, Tsutsumi M, Haraoka J, Hirano K, BeppuM. Photodynamic therapy in combination with talaporfin sodium induces mitochondrial apoptotic cell death accompanied with necrosis in glioma cells. *Biol Pharm Bull*. 2013;36(2):215-21. doi: 10.1248/bpb.b 12-00567. Epub 2012 Nov 29. PMID: 23196427
12. Miki Y, Akimoto J, Hiranuma M, Fujiwara Y. Effect of talaporfin sodium-mediated photodynamic therapy in cell death modalities in human glioblastoma T98G cells. *J Toxicol Sci.* 2014;39(6):821-7. doi: 10.2131/jts.39.821.PMID: 25374373
13. Miki Y, Akimoto J, Moritake K, Hironaka C, Fujiwara Y. Photodynamic therapy using talaporfin sodium induces concentration-dependent programmed necroptosis inhuman glioblastoma T98G cells. *Lasers Med Sci*. 2015 Aug;30(6):1739-45. doi: 10.1007/s10103-015-1783-9. Epub 2015 Jun 25.PMID: 26109138
14. Ichikawa M, Akimoto J, Miki Y, Maeda J, Takahashi T, Fujiwara Y, Kohno M. Photodynamic therapy with talaporfin sodium induces dose-and time-dependent apoptotic cell death in malignant meningioma HKBMM cells. *Photodiagnosis Photodyn Ther*. 2019 Mar; 25: 29-34. doi: 10.1016/j.pdpdt.2018.10.022. Epub 2018 Oct 31.PMID: 30389626
15. Akimoto J. Photodynamic therapy for malignant brain tumors. *Neurol Med Chir (Tokyo)*. 2016; 56: 151-7.
16. Akimoto J, Haraoka J, Aizawa K. Preliminary clinical report on safety and efficacy of photodynamic therapy using talaporfin sodium for malignant gliomas. *Photodiagnosis Photodyn Ther*. 2012; 9: 91-99.
17. Muragaki Y, Akimoto J, Maruyama T, Iseki H, Ikuta S, Nitta M, Maebayashi K, Saito T, Okada Y, Kaneko S, Matsumura A, Kuroiwa T, Karasawa K, Nakazato Y, Kayama T. Phase II clinical study on intraoperative photodynamic therapy with talaporfin sodium and semiconductor laser in patients with malignant brain tumors. *J Neurosurg*. 2013;119, 845-852.
18. Nitta M, Muragaki Y, Maruyama T, Iseki H, Komori T, Ikuta S, Saito T, Yasuda T, Hosono J, Okamoto S, Koriyama S, Kawamata T. Role of photodynamic therapyusing ta laporfin sodium and a semiconductor laser in patients with newly diagnosedglioblastoma. *J Neurosurg*. 2018; 131: 1361-1368. doi: 10.3171/2018.7.JNS18422.

 doi:10.20944/preprints202506.1080.v1

19. Yu CH, Yu CC. Photodynamic therapy with 5-aminolevulinic acid (ALA) impairs tumor initiating and chemo-resistance property in head and neck cancer-derived cancer stem cells. *PLos One* 2014; 9: e87129.
20. Fujishiro T, Nonoguchi N, Pavliukov M, Ohmura N, Kawabata S, Park Y, Kajimoto Y, Ishikawa T, Nakano I, Kuroiwa T. 5-Aminolevulinic acid-mediated photodynamic therapy can target human glioma stem-like cells refractory to antineoplastic agent. *Photodiagnosis Photodyn Ther*. 2018 Dec;24:58-68. doi: 10.1016/j.pdpdt.2018.07.004. Epub 2018 Jul 7.PMID: 29990642
21. Wakimoto H, Kesari S, Farrell CJ, Curry WT Jr, Zaupa C, Aghi M, Kuroda T, Stemmer- Rachamimov A, Shah K, Liu TC, Jeyaretna DS, Debasitis J, Pruszak J, Martuza RL, Rabkin SD. Huma glioblastoma-derived cancer stem cells: establishment of invasive glioma models and treatment with oncolytic virus vectors. *Cancer Res.* 2009; 69(8): 3472-81. doi: 10.1158/0008-5472.CAN-08-3886. Epub 2009 Apr 7.PMID: 19351838.
22. Wakimoto H, Mohapatra G, Kanai R, Curry WT Jr, Yip S, Nitta M, Patel AP, Barnard ZR, Stemmer-Rachamimov AO, Louis DN, Martuza RL, Rabkin SD. Maintenance of primary tumor phenotype and genotype in glioblastoma stem cells. *Neuro Oncol*. 2012; 14(2): 132-44. doi: 10.1093/neuonc/nor195. Epub 2011 Nov 7.PMID: 22067563.
23. Fujimoto Y, Fujita Y, Tanaka K, Nagashima H, Yamanishi S, Ikeuchi Y, Iwahashi H, Sanada S, Muragaki Y, Sasayama T. Clinical benefits of photodynamic therapy using talaporfin sodium in patients with isocitrate dehydrogenase-wildtype diagnosed. glioblastoma: A retrospective study of 100 cases. *Neurosurg* 2024; 1-12. 10.1227/neu.0000000000003247,November 2024. | *DOI:* 10.1227/neu.0000000000003247
24. Chen L, Chaichana KL, Kleinberg L, Ye X, Quinones-Hinojosa A, Redmond K. Glioblastoma recurrence patterns near neural stem cell regions. *Radiother Oncol*. 2015; 116(2): 294-300.
25. Jafri NF. Relationship of glioblastoma multiforme to the subventricular zone is associated with survival. *Neuro Oncol*. 2013; 15: 91-96.
26. Lim DA, Cha S, Mayo MC, Chen MH, Keles E, VandenBerg S, Berger MS. Relationship of glioblastoma multiforme to neural stem cell region predicts invasive and multifocal tumor phenotype. *Neuro Oncol*. 2007; 9: 424-9. doi: 10.1215/15228517-2007-023. Epub 2007 Jul 10.PMID: 17622647.
27. Kobayashi T, Miyazaki M, Sasaki N, Yamamuro S, Uchida E, Kawauchi D, Takahashi M, Otsuka Y, Kumagai K, Takeuchi S, Toyooka T, Otani N, Wada K, Narita Y, Yamaguchi H, Muragaki Y, Kawamata T, Mori K, Ichimura K, Tomiyama A. Enhanced malignant phenotypes of glioblastoma cells surviving Npe6-mediated photodynamic therapy are regulated via ERK1/2 activation. *Cancers (Basel)*. 2020 Dec 4;12(12):3641. doi: 10.3390/cancers12123641.PMID: 33291680.
28. Riss TL, et al. Cell viability assays. In: Markossian S, Grossman A, et al., editors. Assay Guidance Manual [Internet]. Bethesda (MD): Eli Lilly & Company and the National Center for Advancing Translational Sciences; 2013.
29. van Tonder A, Joubert AM, Cromarty AD. Limitations of the 3-(4,5 dimethylthiazol-2-yl)-2,5-diphenyltetrazolium bromide (MTT) assay when compared to three commonly used cell enumeration assays. *BMC Research Notes*. 2015;8:47. doi:10.1186/s13104-015-1000-8
30. Merlin JL, et al. Measurement of cytotoxicity by MTT assay. *Cancer Detection and Prevention*. 1987;10(4–5): 379–385.
31. Abdel-Kader MH, Stepp H, Aniogo EC, Abrahamse H. In vitro study for photodynamic therapy using Fotolon® in glioma cells. *Proc SPIE*. 2015;9542:95420B. doi:10.1117/12.2183815
32. Hamid A, Stepp H, Abdel-Kader MH. LD50 determination in glioma cell lines via MTT following PDT. *Proc SPIE*. 2015;9542:95420B.
33. Choi Y, Kim H, Lee H, Lee J, Kim K, Hasan T, et al. Enhanced efficacy of photodynamic therapy by inhibiting ABCG2 in colon cancer cells. *BMC Cancer*. 2015;15:109. doi:10.1186/s12885-015-1100-5

 doi:10.20944/preprints202506.1080.v1

34. Freeman HS, Golub M. Photodynamic therapy: the development of new photosensitizers. *In: Photodynamic Therapy: Methods and Protocols*. Humana Press, 2010.
35. Chen X, Zhong Z, Xu Z, Chen L, Wang Y. 2′,7′-Dichlorodihydrofluorescein as a fluorescent probe for reactive oxygen species measurement: forty years of application and controversy. *Free Radic Res*. 2010; 44: 587–604.
36. Wrona M, Patel KB, Wardman P. The roles of thiol-derived radicals in the use of 2,7-dichlorodihydrofluorescein as a probe for oxidative stress. *Free Radic Biol Med*. 2008; 44: 56–62.
37. Setsukinai K, Urano Y, Kakinuma K, Majima HJ, Nagano T. Development of novel fluorescence probes that can reliably detect reactive oxygen species and distinguish specific species. *J Biol Chem*. 3004; 278: 3170–3175.
38. Yu D, Zha Y, Zhong Z, Hou S. Improved detection of reactive oxygen species by DCFH-DA: New insight into self-amplification of fluorescence signal by light irradiation. *Sensors and Actuators B: Chemical*. 2021;329:129246. https://doi.org/10.1016/j.snb.2020.129246
39. Li KT, Chen Q, Wang DW, Bai DQ. Mitochondrial pathway and endoplasmic reticulum stress participate in the photosensitizing effectiveness of AE-PDT in MG63 cells. *Photodiagnosis and Photodynamic Therapy*. 2016;13:204–210. https://doi.org/10.1016/j.pdpdt.2015.10.011
40. Zhang R, Fan Q, Yang M, Cheng K, Lu X, Zhang L, et al. Engineering a ROS-responsive nanoplatform for synergistic photodynamic and chemotherapy. *Frontiers in Chemistry*. 2018;6:647. https://doi.org/10.3389/fchem.2018.00647
41. Zhao L, Zhang Y, Sun W, Zhang J, Chen X. Secondary ROS mediate PDT-induced mitochondrial dysfunction in glioma. Journal of Cellular and Molecular Medicine. 2023;27(4):2456–2468.https://doi.org/10.1111/jcmm.17778
42. Sahu A, Kasoju N, Bora U. Fluorescence based detection of intracellular ROS in living cells. *Micron*. 2020;101:41–49. https://doi.org/10.1016/j.micron.2017.09.003
43. Yang W, Wang C, Xu H, Sun J, Liu J, Liu H, et al. Photodynamic therapy induces secondary oxidative stress in cancer cells. Cancer Letters. 2016;370(2):345–356. https://doi.org/10.1016/j.canlet.2015.11.021
44. Liu L, Zhang Z, Xing D. Cell death via mitochondrial apoptotic pathway due to activation of Bax by lysosomal photodamage. *Free Radic Biol Med*. 2011; 51 (1): 53-68.
45. Ormond AB, Freeman HS. Dye Sensitizers for Photodynamic Therapy. *Materials*. 2013; 6 (3): 817-840.
46. Ormond AB, Freeman HS. Dye Sensitizers for Photodynamic Therapy. *Materials*. 2013; 6 (3): 817-840.
47. Heddleston JM, Li Z, McLendon RE, Hjelmeland AB, Rich JN. The hypoxic microenvironment maintains glioblastoma stem cells and promotes reprogramming towards a cancer stem cell phenotype. *Cell Cycle*. 2009; 8(20): 3274-84.
48. Shi T, Zhu J, Zhang X, Mao X. The role of hypoxia and cancer stem cells in development of glioblastoma. *Cancers (Basel)*. 2023; 15: 2613. https://doi.org/10.3390/cancers15092613.
49. Dixit D, Prager BC, Gimple RC, Poh HX, Wang Y, Wu Q, Qiu Z, Kidwell RL, Kim LJY, Xie Q, Vitting-Seerup K, Bhargava S, Dong Z, Jiang L, Hamerlik P, Jaffrey SR, Zhao JC, wang X, Rich JN. The RNA m6A reader YTHDF2 maintains oncogene expression and Is a targetable dependency in glioblastoma stem cells. *Cancer Discov*. 2021; 11: 480–499.
50. Beck TJ, Kreth FW, Beyer W, Mehrkens JH, Obermeier A, Stepp H, Stummer W, Baumgartner R. Interstitial photodynamic therapy of nonresectable malignant glioma recurrence using 5-aminolevulinic acid induced protoporphyrin IX. *Laser Surg Med*. 2007; 39: 386-393.
51. Lietke S, Schmutzer M, Schwartz C, Weller J, Siller S, Aumiller M, Heckl C, Forbrig R, Niyazi M, Egensperger R, Stepp H, Sroka C, Tonn JC, Ruhm A, Thon N. Interstitial photodynamic therapy using 5-ALA for malignant glioma recurrence. *Cancers (Basel)*. 2021; 13: 1767. http://doi.org/10.3390/cancers13081767.
52. McIlroy DR, Shotwell MS, Lopez MG, Vaughn MT, Olsen JS, Hennessy C, Wanderer JP, Semler MS, Rice

 doi:10.20944/preprints202506.1080.v1

TW, Kheterpal S, Billings FT IV. Oxygen administration during surgery and postoperative organ injury: observational cohort study. *BMJ*. 2022; 379: e070941. doi: 10.1136/bmj-2022-070941.